Hybrid Materials

Hybrid Film from Nickel Oxide and Oxygenated Carbon Nanotube as Flexible Electrodes for Pseudocapacitors

Zhong Wu,[a, b] Lin Li,[a, b] Xiao-lei Huang,[a, b] Xin-bo Zhang,[b] and Jun-min Yan*[a]

Abstract: Nanomaterials based on nickel oxide (NiO) have been proposed as one of most promising electrode materials for high-performance supercapacitors. However, their limited electrical conductivity leads to low specific capacitance and unsatisfactory cycling stability. In addition, traditional electrode preparation affects their electrochemical performances. Here, we develop a facile and effective strategy to fabricate hybrid films from NiO and oxygenated carbon nanotubes (OCNT) by filtration. The hybrid film is directly used for electrodes in electrochemical investigations and reveals superior electrochemical properties. By optimizing the ratio of two species; the as-obtained hybrid film electrode exhibits a high specific capacitance, good rate capability and considerable energy density. The superiority can be contributed to the synergistic effect of two species.

Supercapacitors (SCs), also known as electrochemical capacitors or ultracapacitors have attracted tremendous attention due to their fast charge–discharge rates, long and stable cycling life, and relatively simple configuration.[1] Based on different energy-storage mechanisms and electrode materials, SCs can be categorized into electrochemical double layer capacitors (EDLCs) and pseudocapacitors (PCs).[2] EDLCs store electrical energy at the interface of electrode and electrolyte through ion adsorption, which is near physical processes. Electrode materials used for EDLCs are usually carbon-based nanomaterials with high surface area and/or suitable pore structure. In general, EDLCs can provide ultrahigh power density and long cycling life, but limited energy density. On the contrary, PCs can exhibit enhanced energy density by introducing reversible redox reactions on the surface of active materials. Pseudocapacitive materials can mainly be classified as metal oxides/hydroxides, conducting polymers, and so on.[3] However, PCs show improved specific capacitances and energy density, although at the expense of a considerable power density and cycling stability. For optimizing the properties of PCs, hybrid materials with EDLCs-based materials are considered as a promising effective strategy to achieve superior electrochemical performances by combining Faradaic with non-Faradaic processes.[4]

Much effort has been devoted to the research of metal oxides which can provide a variety of oxidation states for fast surface redox reactions. Nickel oxide (NiO) has been intensively studied as one of most promising electrode materials for high-performance PCs due to its intrinsic properties, such as high chemical/thermal stability, ready availability, and low cost.[5] However, it is still far from satisfactory capacitive performance due to its poor electrical conductivity and large volume change during the cycling process. Hence, it is still a challenge to use the high electrochemical capacitive performance of NiO with increased specific capacitances and an enhanced energy density.

Extensive efforts have been dedicated to aspects of materials design and electrode configuration. On one hand, materials design is critical since the electrochemical performances are primarily affected by the intrinsic properties of materials such as surface area and electrical conductivity.[6] Intensive explorations have focused on constructing NiO nanostructures and incorporating NiO with conductive carbonaceous materials such as carbon nanotubes (CNTs). First, nanosized NiO can offer a large specific surface area allowing enough contact area between the electroactive materials and the electrolyte for effective ion transportation.[7] Second, NiO films have been fabricated to improve the pseudocapacitive performances of NiO-based materials by combining with carbon materials.[8] The superiority of NiO/carbon composites can be attributed to the inclusion of carbon materials which can not only disperse NiO to expose more active sites but also improve the electrical conductivity for fast electron transportation. CNTs have been regarded as alternative conductive substrates due to their high conductivity and stable electrochemical behavior.[9] As a result, nanostructured NiO/CNTs can be expected to exhibit enhanced specific capacitance due to their advanced surface area and electrical conductivity which facilitate the full utilization of NiO-based materials.

[a] Z. Wu, L. Li, Dr. X.-l. Huang, Prof. Dr. J.-m. Yan
Key Laboratory of Automobile Materials
Ministry of Education and School of Materials Science and Engineering
Jilin University
Changchun 130012 (P.R. China)
E-mail: junminyan@jlu.edu.cn

[b] Z. Wu, L. Li, Dr. X.-l. Huang, Prof. Dr. X.-b. Zhang
State Key Laboratory of Rare Earth Resource Utilization
Changchun Institute of Applied Chemistry
Chinese Academy of Sciences
Changchun 130022 (P.R. China)

On the other hand, electrode configuration plays an important role in electrochemical investigations. Traditional electrodes are composed of the active material, conductive agent, and binders. The poor conductivity of the binder decreases the electrical conductivity of the electrode materials. Consequently, the addition of additive and binder results in reduced energy and power performance.[10] Therefore, flexible additive-free and binder-free electrodes have emerged as a new mechanically robust electrode configuration achieving high specific capacitance. Recently, researchers have been conscious that monolithic design is favorable for improving the performances of the as-prepared electrodes. NiO-based films with monolithic design have been an alternative material for flexible electrodes in pseudocapacitors. CNTs featured with nanotubes are promising loading substrates for fabricating flexible electrodes.[11]

Herein, we propose a facile and effective approach to fabricate hybrid films based on NiO and oxygenated carbon nanotube (OCNT) as illustrated in Figure 1. At first, NiO precursors
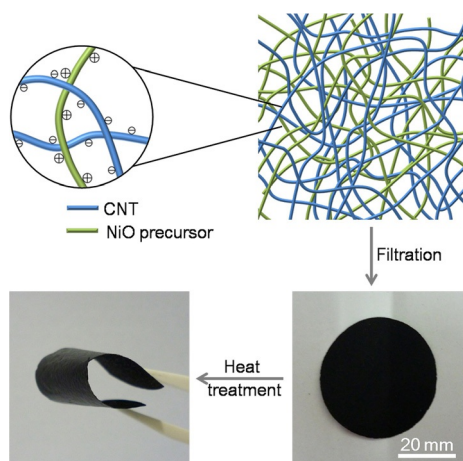
Figure 1. Schematic representation of the synthesis of NiO/OCNT films.

prepared through a template-free hydrothermal process. OCNT is synthesized by oxygenating CNTs in H_2SO_4/HNO_3 (3:1) solution. NiO precursors are anchored on the surface of OCNT through electrostatic interactions between the two species. As a result, NiO precursors are dispersed well and intertwined with nanotubes to form hybrid films with the help of filtration. Followed by a calcination process, the hybrid films based on NiO and OCNT are obtained, which are denoted as the NiO/OCNT films. For comparison, the weight ratio of NiO to OCNT is tuned to determine the effect of OCNT on the electrochemical performances of the hybrid films. In our work, the total masses of composites are firmed as 60 mg when the total area of all electrode films was fixed to ≈ 3.5 cm × 3.5 cm. The ratio of NiO to OCNT is adjusted to be 2:1, 1:1, or 1:2, which are denoted as NiO/OCNT-1, NiO/OCNT-2, and NiO/OCNT-3. The as-prepared NiO/OCNT film (NiO/OCNT-3) shows the highest specific capacitance (686.5 F g^{-1} at 2 mV s^{-1} and 662.1 F g^{-1} at 1 A g^{-1}), benign rate capability (408.2 F g^{-1} at 20 mV s^{-1} and 377.2 F g^{-1} at 20 A g^{-1}) as well as favorable cycling stability (inconspicuous degradation after 1000 cycles).The superior elec-

trochemical properties benefit from the synergistic effect between NiO and CNTs. From a materials design perspective, the presence of CNTs not only improves the conductivity but also prevents the aggregation of NiO nanoparticles. From an electrode configuration perspective, the CNTs enable the formation of hybrid films based on NiO materials. Consequently, more active sites are exposed for redox reactions and thus enhanced properties have been revealed including specific capacitance, rate capability and long-term cycling life. Moreover, this strategy is facile, effective and versatile so that it may be easily extended to other electrode materials.

The crystal structures of the obtained samples are characterized by X-ray diffraction (XRD) pattern. Figure 2a illustrates the
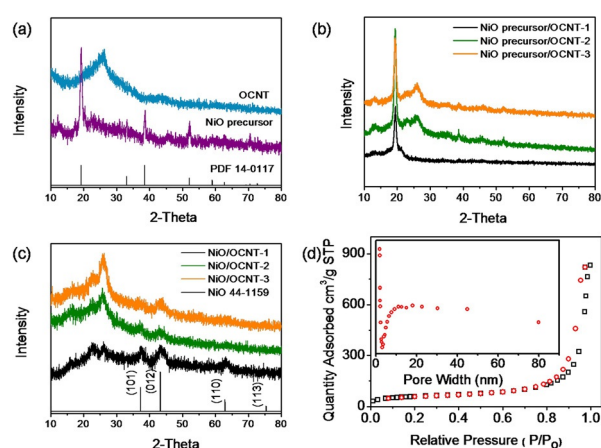
Figure 2. a) XRD patterns of the NiO precursor and OCNT. b) XRD patterns of the NiO precursor/OCNT composites. c) XRD patterns of the NiO/OCNT composites. d) Nitrogen adsorption–desorption isotherm and the pore-size distribution curves (inset) of the NiO/OCNT composite (NiO/OCNT-3).

XRD patterns of NiO precursor and OCNT. The as-prepared NiO precursor can be reasonably assigned to Ni(OH)$_2$ (JCPDS card, NO. 14-0117). When combining with CNTs, there is no significant change as shown in Figure 2b.The 2θ degrees for diffractions of (001), (100), (101), (102), (110) and (111) planes are at 19.258, 33.064, 38.541, 52.100, 59.052, and 62.726°, respectively. Nonetheless, the XRD pattern changes significantly after sintering at 400 °C in air as displayed in Figure 2c. The two diffraction peaks can be referenced to OCNT (2θ values = 26°) and NiO (JCPDS card, NO. 44-1159). The 2θ degrees for diffractions of (101), (012), (110), (104) and (113) planes are at 37.248, 43.286, 62.852, 62.912 and 75.404°, respectively. With the addition of CNTs, it can be found that the crystallization can be optimized with increasing amount of CNTs which results from improved dispersion of NiO on CNTs.

Nitrogen sorption experiments are conducted to investigate the surface area and pore size distribution of NiO/OCNT film, which are generally believed to be critical factors for SCs applications. As shown in Figure 2d, the surface area of NiO/OCNT film (NiO/OCNT-3) is about 195 m^2 g^{-1} calculated by the Brunauer–Emmett–Teller (BET) method. The pore diameter distribution of NiO/OCNT film is estimated from the isotherm adsorption branch using the Barrett–Joyner–Halenda model (inset of

Figure 2 d). The pore sizes are dominated by a narrow distribution of micropores (ca. 3 nm) and a broad distribution ranging from mesopores to macropores. The presence of micropores may be derived from the hollow structure of nanotubes. Besides, the formation of mesopores and macropores is contributed to the dispersion of NiO on OCNT and the network through intertwining nanotubes. These porosity structure can offer more accessible surface area for electrolyte ions and then benefit the electrochemical performances (vide infra).

The morphology and structure of as-prepared samples are investigated by scanning electron microscopy (SEM) and transmission electron microscopy (TEM). Figure 3 a–c and Figure S1
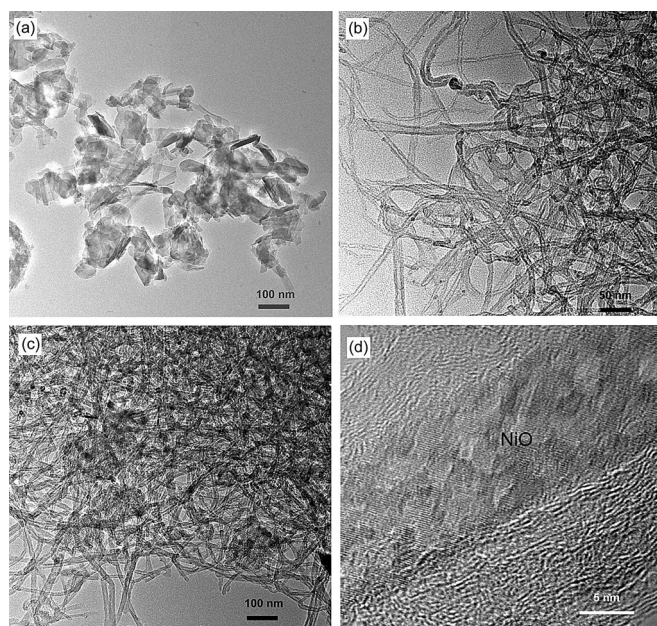
Figure 3. a) TEM image of NiO precursor. b) TEM image of OCNT. c) TEM image of the NiO/OCNT film(NiO/OCNT-3). d) High resolution TEM image of the NiO/OCNT film (NiO/OCNT-3). Scale bars: a) 100 nm, b) 50 nm, c) 100 nm, d) 5 nm.

in the Supporting Information show the TEM and SEM morphology and structure of NiO precursor, OCNT and NiO/OCNT-3, respectively. As shown in Figure 3 a and Figure S1 a, the as-prepared NiO precursors are mixture of nanowire and nanoplates. Figure 3 b and Figure S1 b show the nanotubes of OCNTs. Interestingly, it could be found that the NiO and OCNTs intertwine with each other in Figure 3 c and Figure S1 c to form a network structure. The functional groups of OCNT act as anchoring sites to chelate with NiO procures through electrostatic interaction and then NiO are inlaid in OCNTs network to form a conductive network, which could not only improve the conductivity of NiO but also offer a more accessible channel for ion transport. It is critical for the as-prepared NiO/OCNT film to achieve superior electrochemical performances. The high-resolution TEM image of NiO/OCNT film in Figure 3 d shows lattice fringes of NiO and OCNT, confirming its crystalline nature in accordance with the XRD results in Figure 2 c.

The electrochemical properties of NiO/OCNT films are determined by cyclic voltammetry (CV) to investigate the capacitance mechanism. Figure 4 a–c shows the CV curves of the
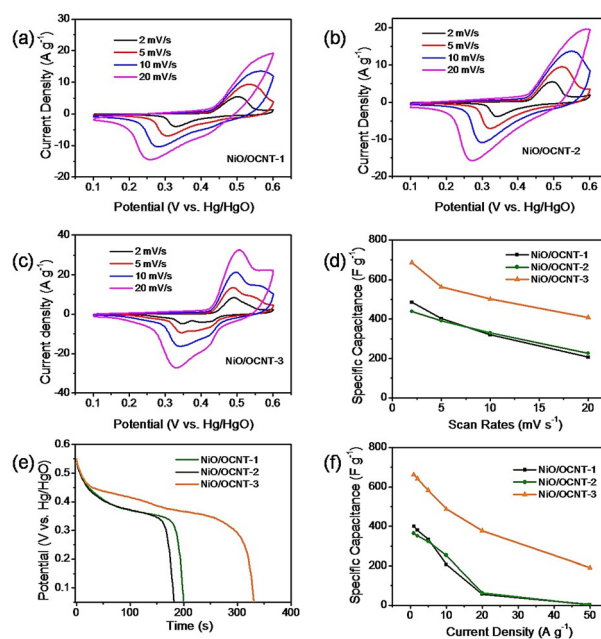
Figure 4. a) CV curves of NiO/OCNT-1 at various scan rates. b) CV curves of NiO/OCNT-2 at various scan rates. c) CV curves of NiO/OCNT-3 at various scan rates. d) Average specific capacitances of the NiO/OCNT composites at various scan rates. e) Galvanostatic discharge curves of the NiO/OCNT composites at 1 A g^{-1}. f) Average specific capacitances of the NiO/OCNT composites at various current densities.

NiO/OCNT composites at different scan rates. Two strong current peaks are observed, indicating that the capacitance of NiO/OCNT films mainly result from pseudocapacitive capacitance based on a fast redox mechanism. The two strong current peaks could be reasonably attributed to the following reaction: $NiO + OH^- = NiOOH + e^-$.[6b] The peak (positive current density) is observed at 0.5 V, indicating an oxidation process, while another peak (negative current density) occurred at 0.35 V, implying a reduction process. These peaks arise from the reversible redox process occurring at the interface of the NiO and the electrolyte during the potential sweep. Comparing the CV curves of three composites, it is obvious that the pseudocapacitive behavior can be optimized with increasing amounts of CNTs, which is a result of the improved dispersion of NiO on CNTs.[7b]

The specific capacitance (Cs, F g^{-1}) values at different scan rate (mV s^{-1}) in the CV measurements are calculated using the following equation:[12]

$$Cs = \frac{\oint I dV}{2\omega v \Delta V},$$

where ΔV (V) is the applied potential window, v is the scan rate, and w (g) is the weight of the active material (2 mg cm^{-2} in this case). The average specific capacitances of the hybrid

Table 1. Specific capacitances [$F\,g^{-1}$] of the NiO/OCNT composites calculated from CV curves.

CV	$2\,mV\,s^{-1}$	$5\,mV\,s^{-1}$	$10\,mV\,s^{-1}$	$20\,mV\,s^{-1}$
NiO/OCNT-1	484.5	402.2	319.9	206.1
NiO/OCNT-2	438.4	390.4	329.1	225.9
NiO/OCNT-3	696.5	562.8	501	468.2

films are illustrated in Figure 4d and Table 1. The NiO/OCNT-3 film displays higher specific capacitances than those of NiO/OCNT-1 film and NiO/OCNT-2 film at various scan rates. At a low scan rate of $2\,mV\,s^{-1}$, the NiO/OCNT-3 film can achieve a high specific capacitance value of $686.5\,F\,g^{-1}$ whereas lower value of $484.5\,F\,g^{-1}$ and $438.4\,F\,g^{-1}$ for NiO/OCNT-1 film and NiO/OCNT-2 film, respectively. At a high scan rate of $20\,mV\,s^{-1}$, the specific capacitance of NiO/OCNT-3 film still retain a relative value of $468.2\,F\,g^{-1}$ indicating their good rate capability. According to the equation: $E = 1/2\,CV^2$ (V is the applied potential window, C is the specific capacitance), the highest energy density of NiO/OCNT-3 film can be calculated as $23.8\,Wh\,kg^{-1}$, which is comparable to the electrochemical properties of RuO_x in previous reports.[13] Moreover, the specific energy density based on the total mass (NiO + CNT) can achieve $5.95\,Wh\,kg^{-1}$.

Galvanostatic discharge curves (GC) are also employed to further confirm the specific capacitances of the NiO/OCNT composites, which are shown in Figure 4e and Figure S2. Figure 4e shows the GC curves of the NiO/OCNT composites at the current density of $1\,A\,g^{-1}$. The electrochemical properties of NiO/OCNT-3 film are superior to those of NiO/OCNT-1 film and NiO/OCNT film, which is in accordance with CV results. Specific capacitance could be calculated from the galvanostatic discharge curve, using the following equation:[12]

$$C = \frac{I\Delta t}{m\Delta V},$$

Where I is discharge current, Δt is the time for a full discharge, m indicates the mass of the active material, and ΔV represents the voltage change after a full discharge. As shown in Figure 4f and Table 2, the specific capacitances at $1\,A\,g^{-1}$ are 363.5, 399.7 and $662.1\,F\,g^{-1}$ for NiO/OCNT-1 film, NiO/OCNT-2 film and NiO/OCNT-3 film, respectively. Even at the high current density of $50\,A\,g^{-1}$, the NiO/OCNT-3 film performs a high specific capacitance of $190.6\,F\,g^{-1}$ while the specific capacitances of the NiO/OCNT-1 film and NiO/OCNT-2 film are less than $5\,F\,g^{-1}$.

For comparison, Table 1 and Table 2 summarize the specific capacitances of NiO/OCNT-1, NiO/OCNT-2, and NiO/OCNT-3 films calculated from CV curves and galvanostatic discharge curves. We can discover some phenomena from these results. First, all hybrid films show higher specific capacitance at low scan rates or current density than that of high scan rates or current density. Moreover, it is found that the specific capacitances of NiO/OCNT-1 and NiO/OCNT-2 are much lower than those of the NiO/OCNT-3 film at all tested conditions, providing another evidence for the superiority of the NiO/OCNT-3 film. Several reasons can account for these results as following. First, the carbon nanotubes act as a conductive scaffold, which enhances the electrical conductivity of NiO. Second, the films are directly used as a pseudocapacitive electrode, which reduces the diffusion length and enhanced the electrical conductivity. Third, the porous structure resulting from overlapped nanotubes provide porous channels for fast transport of electrolyte ion. Fourth, more redox reactions are conducted on the surface of films at the low scan rates or current density and then higher specific capacitance can be obtained. Fifth, the NiO/OCNT-3 films are composed by a larger amount of CNTs than that of the NiO/OCNT-1 film and NiO/OCNT-2 film. They can obtain better dispersion of NiO on CNTs which further expose more active sites to improve the specific capacitance and rate capability. Consequently, superior electrochemical properties of NiO/OCNT-3 film are reached including the specific capacitances and rate capability.

For practical application, cycling stability is crucial for an electrode material to be used in electrochemical capacitors. To investigate the cycling stability of the as-prepared NiO/OCNT film electrodes, we performed CV tests for 1000 times between 0.1 and 0.6 V at the scan rate of $20\,mV\,s^{-1}$. The CV curves as a function of cycle number are plotted in Figure 5a. It is found that all the NiO/OCNT film electrodes exhibit good cycling stability after 1000 cycles. For the NiO/OCNT-1 and NiO/OCNT-2 films, the degradation of specific capacitance are 10.2% and 18.1% after 1000 cycles, respectively. Especially, the NiO/OCNT-3 film displays excellent cycling stability with no obvious deg-

Table 2. Specific capacitances [$F\,g^{-1}$] of the NiO/OCNT composites calculated from galvanostatic discharging curves.

GC	$1\,A\,g^{-1}$	$5\,A\,g^{-1}$	$10\,A\,g^{-1}$	$50\,A\,g^{-1}$
NiO/OCNT-1	399.7	333.3	205.9	3.3
NiO/OCNT-2	363.5	322.4	252.8	0.5
NiO/OCNT-3	662.1	582.4	487.4	190.6
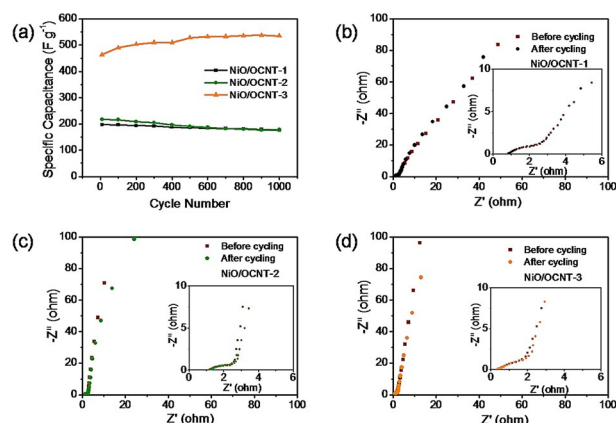
Figure 5. a) Cycling stability of the NiO/OCNT composites at $20\,mV\,s^{-1}$. b) EIS data of NiO/OCNT-1 before and after cycling. c) EIS data of NiO/OCNT-2 before and after cycling. d) EIS data of NiO/OCNT-3 before and after cycling (insets are enlarged plots).

radation after 1000 cycles. The outstanding capacitive behavior further demonstrates the superiority of the hybrid films. On one hand, the long-term stability is attributed to the intimate bindings of NiO and OCNT affording facile electron transports.[7d] On the other hand, excellent cycling stability is promoted by the presence of carbon nanotubes, which retard the large volume change of NiO-based materials during the cycling process.[8a] Furthermore, it is worth noting that a slight increase is observed before 500 cycles and then the tendency holds nearly stable until 1000 cycles. The slight increase may be attributed to the improvement of ion accessibility involving more exposed active surface area.

In addition, electrochemical impedance spectroscopy (EIS) is conducted to investigate the transport characteristics of the charge carriers within the as-prepared film electrodes using a Nyquist plot, which represents the imaginary part ($-Z''$) and real part (Z') of impedance. Figure 5b–d show Nyquist plots of the three types of NiO/OCNT film electrodes before and after 1000 cycles. The impedance spectra consist of one semicircle at high frequency, followed by a straight line at the low frequency range. The high frequency semicircle intercepts the real axis at R_s and ($R_s + R_{ct}$). R_s means a bulk solution resistance which is related to several aspects including the electrolyte resistance, the collector/electrode contact resistance, and the electrode/electrolyte interface resistance. R_s displays no obvious distinction for all NiO/OCNT film electrodes before and after cycling. The NiO/OCNT-3 film electrode exhibits the lowest bulk solution resistance with the R_s value of 0.415 ohm. R_s values for the NiO/OCNT-1 film and NiO/OCNT-2 film electrodes are 0.897 ohm and 1.252 ohm, respectively. R_{ct} means a charge-transfer resistance, which is calculated from the radius of the semicircle. R_{ct} display no obvious distinction for all NiO/OCNT film electrodes before and after cycling. The NiO/OCNT-3 film electrode exhibits the lowest charge-transfer resistance with the R_{ct} value of 0.25 ohm. R_s values for the NiO/OCNT-1 film and NiO/OCNT-2 film electrodes are 0.91 ohm and 0.599 ohm, respectively. The inclined portion of the curve in the low frequency is ascribed to the Warburg impedance, which is related to ion diffusion/transport in the electrolyte. The more vertical shape before cycling indicates a better capacitive behavior of the electrode.

We can summarize the EIS spectra to analyze and verify the results of cycling stability. In terms of R_s and R_{ct}, We can note that there is no obvious distinction for the NiO/OCNT film electrodes before and after cycling, which demonstrate their good cycling stability. The lowest resistance of the NiO/OCNT-3 film electrode further evidences its superiority to other film electrodes. In terms of the Warburg impedance, negligible deviation of the NiO/OCNT film electrodes before and cycling indicate their excellent cycling stability. The resultant EIS analysis is in accordance with the cycling stability investigation.

In summary, we have developed a facile and effective strategy to successfully fabricate hybrid films from NiO and oxygenated carbon nanotubes through electrostatic interactions. The hybrid films can be directly used as electrode materials in electrochemical investigation. This strategy not only reduces the complicated and time consuming electrode preparation pro-

cess but also improves their capacitive performances resulting from enhance electrical conductivity and monolithic design. The electrochemical performances are affected by the ratio of NiO and OCNT. Interestingly, the as-prepared NiO/OCNT films show superior electrochemical performances including specific capacitances, rate capability and cycling stability. A highest specific capacitance of 686.5 F g^{-1} is achieved by optimizing the ratio. Synchronously, the film electrode exhibits a comparable energy density of 23.8 Wh kg^{-1} to the electrochemical properties of RuO$_x$. The superiority of the hybrid film electrode can be contributed to the synergistic effects between OCNT and NiO. First, the carbon nanotubes act as conductive scaffold, which enhances the electrical conductivity of NiO. Second, the films are directly used as a pseudocapacitive electrode, which reduces the diffusion length and enhances the electrical conductivity. Third, the porous structure resulting from overlapped nanotubes provides porous channels for fast transport of electrolyte ions. Fourth, NiO is dispersed well on the surface of CNTs, thus more active sites are exposed for full utilization of NiO. Fifth, intimate bindings of NiO and OCNT afford facile electron transport. Sixth, the presence of CNTs retards the large volume change of NiO-based materials during the cycling process. Consequently, the hybrid film electrodes reveal superior capacitive performances. This strategy is facile, effective and versatile so it may be easily extended to other electrode materials. The obtained excellent performance opens up new opportunities in the development of high-performance pseudocapacitors.

Experimental Section

Preparation of NiO precursor: First, 2.5759 g of nickel sulfate (NiSO$_4$·6H$_2$O) and 0.196 g of sodium hydroxide (NaOH) were dissolved in 20 mL deionized (DI) water under continuously stirring, respectively. Then the two solutions were mixed and stirred for 10 min, the as-obtained precipitation was washed with DI water once and then the subsequent solution was transferred to a 50 mL Teflon-lined stainless steel autoclave for a hydrothermal reaction at 120 °C for 24 h. Finally, NiO precursor was washed with DI water and ethanol by centrifugal cleaning three times.

Preparation of acid-treated oxygenated CNT: CNTs were placed into 15 mL mixture of nitric acid and sulfuric acid (with a ratio of 1:3) under reflux at 70 °C for 2 h, and then were washed by DI water several times to obtain the acid-treated oxygenated CNTs (OCNT).

Preparation of NiO/OCNT paper electrodes: 40 mg of the as-prepared NiO precursor powders were homogenously dispersed in 50 mL DI water and subsequently mixed with OCNT suspension (with 20 mg of OCNTs in 20 mL DI water). The mixture of NiO precursor and OCNT were stirred for 30 min to ensure fully interpenetration of OCNT and NiO precursor. Then a NiO/OCNT precursor film was prepared after vacuum filtration and freeze drying treatment of the OCNT and NiO precursor mixture. Finally, the NiO/OCNT paper was obtained after heat treatment NiO/OCNT precursor film at 400 °C in air for 2 h. For comparison, other composites with different ratio of NiO and OCNT were also prepared. In our work, the total mass of composites was fixed at 60 mg, and then the ratio of NiO to OCNT was adjusted to 2:1, 1:1, or 1:2, which were denoted as NiO/OCNT-1, NiO/OCNT-2, and NiO/OCNT-3.

Electrochemical measurements: The electrochemical measurements were carried out using a three-electrode mode in 6 M KOH aqueous solution. Hg/HgO electrode filled with 1 M KOH was used as reference electrode and a platinum plate was used as counter electrode. The NiO/OCNT paper was directly used as electrodes without adding any other polymeric binders or conductive additives. The sizes of all electrode films were fixed to ≈ 1.0 cm $\times$ 1.0 cm, and the areal mass loading of NiO/OCNT paper was 2.0 mg cm^{-2}. Two Ni foams were used as current collectors. Electrochemical studies including cyclic voltammetry (CV), galvanostatic charge–discharge (GC) and electrochemical impedance spectroscopy (EIS) were carried out using VMP3 electrochemical workstation (Bio-logic Inc.). All tests were performed at room temperature. Typical CV curves were measured at different scan rates from 2 to 20 mV s^{-1} between 0.1 and 0.6 V (vs Hg/HgO). GC measurements were conducted under various current densities from 1 to 50 A g^{-1} between 0.05 and 0.55 V (vs Hg/HgO). EIS tests were performed for the working electrode in a frequency range of 100 kHz–0.01 Hz with ac perturbation of 10 mV. The EIS data were analyzed using Nyquist plots, which represent the imaginary part (Z′′) and real part (Z′) of impedance.

Acknowledgements

[1] a) P. Simon, Y. Gogotsi, *Nat. Mater.* **2008**, *7*, 845–854; b) M. D. Stoller, R. S. Ruoff, *Energy Environ. Sci.* **2010**, *3*, 1294–1301; c) G. Wang, L. Zhang, J. Zhang, *Chem. Soc. Rev.* **2012**, *41*, 797–828; d) A. Ghosh, Y. H. Lee, *ChemSusChem* **2012**, *5*, 480–499.

[2] a) H. Wang, H. Dai, *Chem. Soc. Rev.* **2013**, *42*, 3088–3113; b) Y. Wang, Y. Xia, *Adv. Mater.* **2013**, *25*, 5336–5342; c) N. S. Choi, Z. Chen, S. A. Freunberger, X. Ji, Y. K. Sun, K. Amine, G. Yushin, L. F. Nazar, J. Cho, P. G. Bruce, *Angew. Chem. Int. Ed.* **2012**, *51*, 9994–10024; *Angew. Chem.* **2012**, *124*, 10134–10166; d) I. E. Rauda, V. Augustyn, B. Dunn, S. H. Tolbert, *Acc. Chem. Res.* **2013**, *46*, 1113–1124.

[3] a) V. Augustyn, P. Simon, B. Dunn, *Energy Environ. Sci.* **2014**, *7*, 1597–1614; b) C. Liu, F. Li, L. P. Ma, H. M. Cheng, *Adv. Mater.* **2010**, *22*, E28–E62; c) H. Jiang, P. S. Lee, C. Li, *Energy Environ. Sci.* **2013**, *6*, 41–53; d) Q. Lu, J. G. Chen, J. Q. Xiao, *Angew. Chem. Int. Ed.* **2013**, *52*, 1882–1889;

Angew. Chem. **2013**, *125*, 1932–1940; e) B. L. Ellis, P. Knauth, T. Djenizian, *Adv. Mater.* **2014**, *26*, 3368–3397; f) Z. Wu, X. L. Huang, Z. L. Wang, J. J. Xu, H. G. Wang, X. B. Zhang, *Sci. Rep.* **2014**, *4*, 3669.

[4] a) H. Chen, L. Hu, M. Chen, Y. Yan, L. Wu, *Adv. Funct. Mater.* **2014**, *24*, 934–942; b) X. He, N. Zhao, J. Qiu, N. Xiao, M. Yu, C. Yu, X. Zhang, M. Zheng, *J. Mater. Chem. A* **2013**, *1*, 9440–9448; c) J. Zhang, X. S. Zhao, *ChemSusChem* **2012**, *5*, 818–841; d) X. Jia, X. Zhu, Y. Cheng, Z. Chen, G. Ning, Y. Lu, F. Wei, *Small* **2015**, *11*, 3135–3142.

[5] a) L. Fan, L. Tang, H. Gong, Z. Yao, R. Guo, *J. Mater. Chem.* **2012**, *22*, 16376–16381; b) S. K. Meher, P. Justin, G. R. Rao, *ACS Appl. Mater. Interfaces* **2011**, *3*, 2063–2073; c) Q. Lu, M. W. Lattanzi, Y. Chen, X. Kou, W. Li, X. Fan, K. M. Unruh, J. G. Chen, J. Q. Xiao, *Angew. Chem. Int. Ed.* **2011**, *50*, 6847–6850; *Angew. Chem.* **2011**, *123*, 6979–6982; d) R. S. Devan, R. A. Patil, J. H. Lin, Y. R. Ma, *Adv. Funct. Mater.* **2012**, *22*, 3326–3370.

[6] a) M. Liu, J. Chang, J. Sun, L. Gao, *RSC Adv.* **2013**, *3*, 8003–8008; b) J. H. Kim, S. H. Kang, K. Zhu, J. Y. Kim, N. R. Neale, A. J. Frank, *Chem. Commun.* **2011**, *47*, 5214–5216; c) M. S. Wu, Y. R. Zheng, G. W. Lin, *Chem. Commun.* **2014**, *50*, 8246–8248.

[7] a) G. Zhang, L. Yu, H. E. Hoster, X. W. Lou, *Nanoscale* **2013**, *5*, 877–881; b) W. Lv, F. Sun, D. M. Tang, H. T. Fang, C. Liu, Q. H. Yang, H. M. Cheng, *J. Mater. Chem.* **2011**, *21*, 9014; c) D. Su, H. S. Kim, W. S. Kim, G. Wang, *Chem. Eur. J.* **2012**, *18*, 8224–8229; d) B. Wang, J. S. Chen, Z. Wang, S. Madhavi, X. W. D. Lou, *Adv. Energy Mater.* **2012**, *2*, 1188–1192.

[8] a) X. h. Xia, J. p. Tu, X. L. Wang, C. d. Gu, X. b. Zhao, *J. Mater. Chem.* **2011**, *21*, 671–679; b) K. C. Liu, M. A. Anderson, *J. Electrochem. Soc.* **1996**, *143*, 124; c) A. I. Inamdar, Y. Kim, S. M. Pawar, J. H. Kim, H. Im, H. Kim, *J. Power Sources* **2011**, *196*, 2393.

[9] a) C. Biswas, Y. H. Lee, *Adv. Funct. Mater.* **2011**, *21*, 3806–3826; b) Z. Yan, L. Ma, Y. Zhu, I. Lahiri, M. G. Hahm, Z. Liu, S. Yang, C. Xiang, W. Lu, Z. Peng, Z. Sun, C. Kittrell, J. Lou, W. Choi, P. M. Ajayan, J. M. Tour, *ACS Nano* **2013**, *7*, 58–64; c) Y. Jiang, P. Wang, X. Zang, Y. Yang, A. Kozinda, L. Lin, *Nano Lett.* **2013**, *13*, 3524–3530; d) S. W. Lee, B. M. Gallant, Y. Lee, N. Yoshida, D. Y. Kim, Y. Yamada, S. Noda, Y. Shao-Horn, *Energy Environ. Sci.* **2012**, *5*, 5437–5444; e) C. Shuo, S. H. Yang, P. T. Hammond, *J. Am. Chem. Soc.* **2009**, *131*, 671–679.

[10] a) L. Li, Z. Wu, S. Yuan, X. B. Zhang, *Energy Environ. Sci.* **2014**, *7*, 2101–2122; b) X. Wang, X. Lu, B. Liu, D. Chen, Y. Tong, G. Shen, *Adv. Mater.* **2014**, *22*, E28–E62; c) B. Brown, I. A. Cordova, C. B. Parker, B. R. Stoner, J. T. Glass, *Chem. Mater.* **2015**, *27*, 2430–2438.

[11] a) C. J. Shearer, A. Cherevan, D. Eder, *Adv. Mater.* **2014**, DOI: 10.1002/adma.201305254; b) C. Yuan, L. Yang, L. Hou, J. Li, Y. Sun, X. Zhang, L. Shen, X. Lu, S. Xiong, X. W. Lou, *Adv. Funct. Mater.* **2012**, *22*, 2560–2566; c) L. Shen, Q. Che, H. Li, X. Zhang, *Adv. Funct. Mater.* **2013**, DOI: 10.1002/adfm.201303138.

[12] a) J. Yan, Z. Fan, W. Sun, G. Ning, T. Wei, Q. Zhang, R. Zhang, L. Zhi, F. Wei, *Adv. Funct. Mater.* **2012**, *22*, 2632–2641; b) H. Wang, H. S. Casalongue, Y. Liang, H. Dai, *J. Am. Chem. Soc.* **2010**, *132*, 7472–7477.

[13] J. Y. Kim, K. H. Kim, S. B. Yoon, H. K. Kim, S. H. Park, K. B. Kim, *Nanoscale* **2013**, *5*, 6804–6811.